The production process of barium in shale gas flowback water based on ion-exchange kinetics

Xuecheng Zheng[a,b], Wei Luo[a], Nanjun Lai[a,b,c],*

[a]*College of Chemistry and Chemical Engineering, Southwest Petroleum University, Chengdu, China,*
emails: lainanjun@126.com (N. Lai), xc.zheng@swpu.edu.cn (X. Zheng), lw_123wwdn@163.com (W. Luo)
[b]*State Key Laboratory Oil and Gas Reservoir Geology and Exploitation, Chengdu University of Technology, Chengdu, China*
[c]*State Key Laboratory of Molecular Engineering of Polymers, Fudan University, Chengdu, China*

ABSTRACT

Fracturing flowback water contains high concentrations of Ba^{2+}, which cause serious problems when the water is reused and reinjected. Therefore, the study of the production of Ba^{2+} is of great practical significance. For this study, we collected shale mineral samples from a shale gas development zone in China. X-ray diffraction measurement of the samples revealed that their clay minerals are dominated by illite and kaolinite to a lesser degree than minor calcite and that these minerals constitute 50%–60% of the shale minerals. X-ray fluorescence measurement confirmed that the maximum content of Ba is 48.7269% in the shale minerals. By inductively coupled plasma optical emission spectrometer analysis, we find that high-concentration Ba^{2+} is present in the flowback water. The barium ion-exchange capacity is calculated in terms of the ion-exchange model based on the rule of equivalent exchange, and the shrinking core model is presented to investigate the kinetic behaviour of this reaction in the flowback water. The results show that the average exchange capacities of Na^+, K^+, and Ca^{2+} are 53.98%, 35.06%, and 7.15%, respectively, and the ion-exchange process is mainly controlled by liquid film diffusion. We report that the calculated results obtained from the kinetic model agree with the engineering data that indicate that the ion-exchange reaction is the main reason for increased Ba^{2+}.

Keywords: Barium; Exchange; Kinetics; Shale gas

1. Introduction

Shale gas is a type of unconventional, clean, and highly efficient natural gas that is trapped within shale formations. It has become an important source of natural gas worldwide [1]. Hydraulic fracturing is the most popular technology of shale gas development, but the process requires up to 20,000 m^3 of fracturing fluid per well. Of this fluid, 15%–80% may return to the surface as flowback water [2,3]. The flowback water contains high concentrations of organics, chloride, and barium ion, which have different degrees of adverse effects on the reuse of the water. Most of these components come from dissolution. However, the source of Ba^{2+} remains unconfirmed.

Liu and Shaffer demonstrated that fracturing fluid contains a cross-linking agent, thickener, fungicides, acid, and a pH value regulator. Flowback water contains many metal ions (i.e., Ca^{2+}, Mg^{2+}, Ba^{2+}, and Sr^{2+}) [4,5,6]. Renock et al. indicated that part of the source of Ba^{2+} is the ion-exchange reaction with Na^+ and Ca^{2+} (the ion-exchange reactions in underground strata and clay) while another part is water-rock interaction and clay dissolution [7]. Stewart et al. reported that more Ba is associated with cation-exchangeable sites in MS than it is with soluble salts or carbonates [8]. Phan et al. indicated that 9%–74% of the total Ba in MS comprises a cation-exchangeable fraction [9]. Onken et al. showed that Ba^{2+} reacts with K^+ rapidly on kaolinite and montmorillonite [10]. Yang reported that the ion diffusion ability increases with clay mineral content.

* Corresponding author.

High-surface area clay minerals, such as montmorillonite, can greatly enhance the ion diffusion ability in shale reservoirs [11]. Wang found that the amount of calcium and magnesium gradually increases after the chemical reaction between the alkali surfactant polymer solution and the reservoir core [12]. Previous studies have investigated the ion-exchange reaction between solutions with underground strata and clays. The present study considers the ion-exchange mechanism between the shale gas fracturing fluid and underground minerals.

In terms of the solid–liquid ion exchange, Wen described the Mg^{2+}–NH_4^+ exchange process by using the logarithmic empirical model of ion exchange [13]. Li reported the kinetics of the Na^+–Cu^{2+} ion-exchange reaction on Na-pretreated clinoptilolite and identified the rate-determining steps as liquid film diffusion and particle dispersion [14]. Siu investigated the kinetics of the ion-exchange process and tested four kinetic models to verify the removal of copper ions from wastewater by ion exchange [15]. Zeid studied the heavy metal ion-exchange kinetics over the surface of nylon 6,6 Zr(IV) under particle diffusion controlled phenomena [16]. Wu calculated the K^+–Li^+ exchange rate and showed that the rate of the steps is controlled by two or three interactions of liquid film diffusion, particle diffusion, and chemical reaction at the same time as a shrinking core model of ion exchange [17].

This paper discusses the exchange process and proportion of Ba^{2+} based on ion-exchange kinetics, and it analyses the key step of the reaction. The calculated results are comparable with data measured at the engineering site, which provide the theoretical basis for the production of Ba^{2+}.

2. Materials and methods

2.1. Sample collection

We obtained shale mineral samples from the shale gas development zone D2 platform in China, approximately 1.5 m below the surface, to minimize weathering [18]. The core samples were obtained from an excavated area of shale blocks using a fresh dill core. We observed that the surface of the samples was weathered and contained high-concentration Ba. The development zone platform contained 48 fractured segments at a time, and the water consumption per segment ranged from 1,212.17 to 2,564.56 m^3. The total displacement was about 86,758.76 m^3. The backflow rate of the fracturing fluid was 7%–20%.

2.2. Characterization of shale samples

2.2.1. Characterization methods

The mineral compositions of the samples were measured by x-ray diffraction (XRD) type X Pert PRO MPD. The test conditions were Cu target, working voltage 40 kV, working current 30 mA, and step length 0.02°. The method for quantitative analysis of the sample compositions was the *K* value method.

Qualitative analysis of elements of the shale samples and quantitative analysis of the weight percent of these elements were conducted with x-ray fluorescence (XRF) spectrometer type AXIOS. The concentration of major metal cations and nonmetal ions in the fracturing flowback water was measured by inductively coupled plasma optical emission spectrometer

(ICP-OES) type Optima 7,300V, and the fracturing flowback water was taken from a backwater pool at the engineering site.

2.2.2. Characterization results

The XRD patterns confirmed the presence of illite, kaolinite, montmorillonite, and quartz in the shale samples. Fig. 1 shows that the main constituents of shale minerals in the study area are clay mineral and quartz. Quantitative analysis using an internal standard method shows that the shale samples have a mineralogical composition of 42.5% quartz, 26.5% illite, 12.7% kaolinite, 4.6% potash feldspar, and 2.1% calcite. Because of weathering, little montmorillonite is present in the shale minerals.

Major and trace elements for the core samples were measured by XRF and are shown in Table 1. All of the elements came from the rock rather than the drilling muds because there were no drilling muds present in the process to obtain samples. The samples contained many metal ions. As Ba was the prominent mineral, analyzing the trace of Ba is very significant. Although small amounts of Na and Mg were present in the mineral, the K, Ca, and Na content will increase during the dissolution of the water-rock reaction while the Al and Si contents will not be affected.
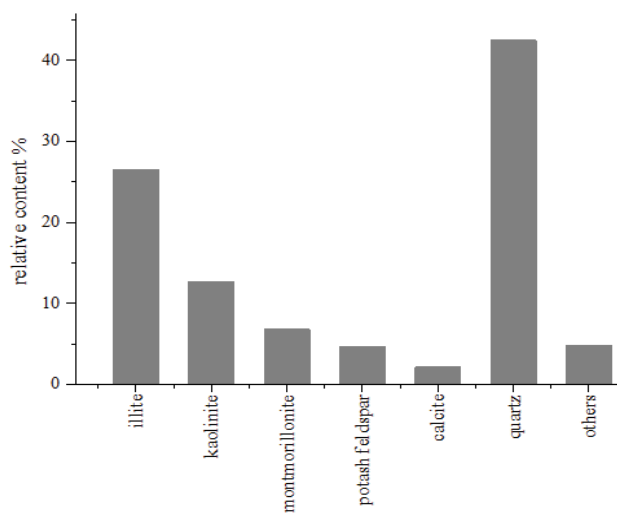
Fig. 1. Results of X-ray diffraction measurement.

Table 1
Results of x-ray fluorescence measurement

Elements	Mass percentage %
K	2.5653
Ca	6.3262
Na	0.6781
Al	7.2136
Si	10.5163
Mg	0.7566
Fe	3.6728
Ba	48.7269
S	2.5675

2.2.3. Engineering data

The tracking analysis for fracturing flowback water in the D2 platform is shown in Fig. 2. Shale gas flowback water is characterized by complicated components, a great variation of water quality, a high concentration of Ba, etc. This study considers the D2 platform as the research object: tracking and measuring the major metal cations (Na, K, Ca, and Ba) in the flowback water from a backwater pool over a period of 25 d. It is not necessary and significant to observe the reverse flow time of the fracturing fluid for more than 26 d because the concentration of each metal cation hardly changed.

2.3. Experimental methods

2.3.1. Description of experimental process

The shale core sample weight of 1 g was added to a high-temperature/high-pressure reactor which can withstand a maximum pressure of 60 MPa. The volume of fracturing fluid in this reactor was 50 mL, and the fracturing fluid for the experiments came from the shale gas development zone

D2 platform in China. The experiments were conducted at an elevated temperature and pressure (90°C, 20 MPa) designed to simulate typical conditions in shale gas wells in China. Meanwhile, the gas in the reactor was maintained with nitrogen to replicate anoxic conditions in the subsurface. The reaction time of the experiments was measured on Days 5, 10, 17, and 25, and the cations in the solution after the reaction were measured with ICP-OES. In addition, a controlled experiment was setup so that the fracturing fluid reacted with the shale core samples at normal temperature and pressure.

2.3.2. The detection results of ICP-OES

The cations in the solution on Days 0, 5, 10, 17, and 25 were detected using ICP-OES. As summarized in Table 2(a), the results show that Ba appeared in the solution on Day 5 and the quantity of Ba increased with the reaction time. The concentrations of Na, K, Ca, and Mg decreased: thus, it was proved that the production of Ba occurred via ion-exchange reaction with the cations of the fracturing fluid. Given the little change in the concentrations of Mg^{2+} over
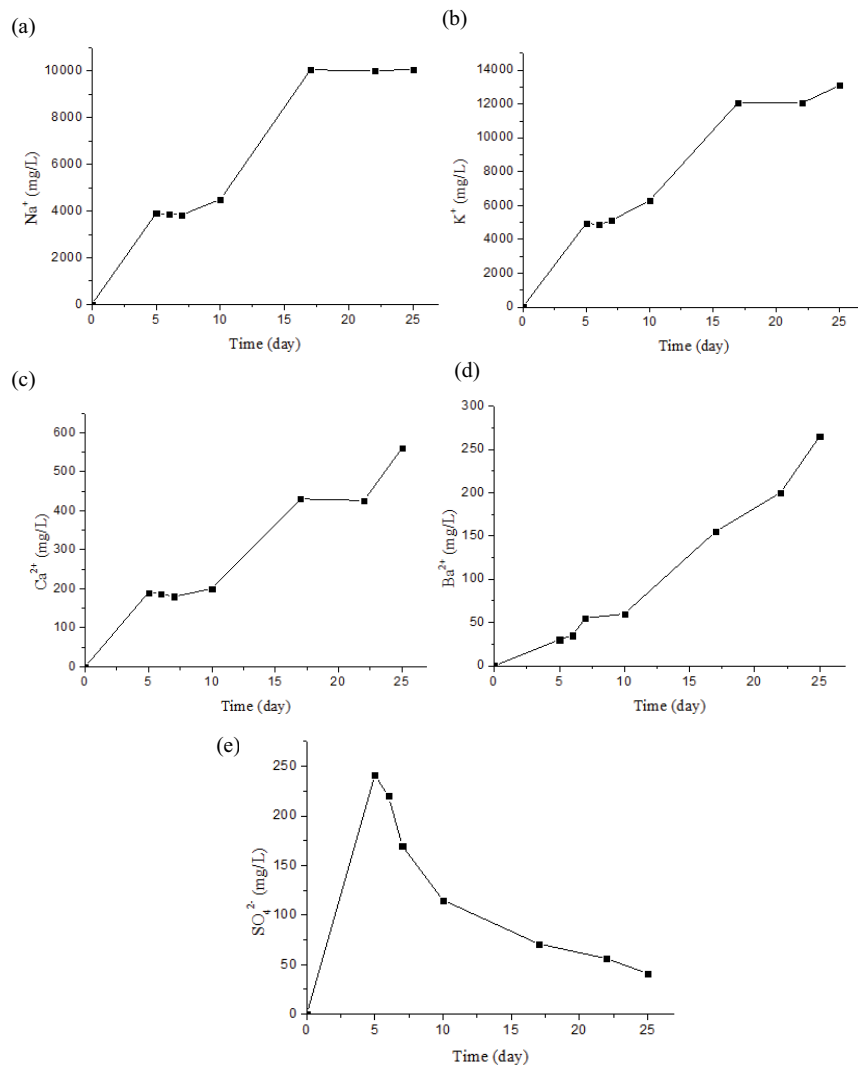
Fig. 2. Variation for different ion concentrations in flowback water for (a) Na^+, (b) K^+, (c) Ca^{2+}, (d) Ba^{2+}, and (e) SO_4^{2-}

Table 2(a)
The detection results of ion-exchange experiment

Time (d)	Na$^+$	Ca^{2+}	K$^+$	Mg^{2+}	Ba^{2+}
	g/mL				
0	2.4113×10^{-3}	1.4765×10^{-4}	3.5672×10^{-3}	1.5325×10^{-4}	0
5	2.5011×10^{-3}	1.6124×10^{-4}	3.6731×10^{-3}	1.5329×10^{-4}	3.5671×10^{-4}
10	2.4715×10^{-3}	1.6115×10^{-4}	3.6326×10^{-3}	1.5321×10^{-4}	3.9563×10^{-4}
17	2.4275×10^{-3}	1.6110×10^{-4}	3.6071×10^{-3}	1.5318×10^{-4}	4.1011×10^{-4}
25	2.3835×10^{-3}	1.6106×10^{-4}	3.5576×10^{-3}	1.5317×10^{-4}	6.4308×10^{-4}

Table 2(b)
The detection results of controlled experiment

Time (d)	Na$^+$	Ca^{2+}	K$^+$	Mg^{2+}	Ba^{2+}
	g/mL				
0	2.4113×10^{-3}	1.4765×10^{-4}	3.5672×10^{-3}	1.5325×10^{-4}	0
5	2.4115×10^{-3}	1.4765×10^{-4}	3.5673×10^{-3}	1.5325×10^{-4}	0
10	2.4113×10^{-3}	1.4766×10^{-4}	3.5673×10^{-3}	1.5326×10^{-4}	0
17	2.4113×10^{-3}	1.4765×10^{-4}	3.5674×10^{-3}	1.5325×10^{-4}	0
25	2.4114×10^{-3}	1.4767×10^{-4}	3.5675×10^{-3}	1.5325×10^{-4}	0

25 d, the ion-exchange reaction between Mg^{2+} and Ba^{2+} could be neglected. Table 2(b) shows the detection results of the controlled experiment. There was nearly no change in the concentrations of the ions on certain days, which indicates that ion-exchange reactions exist between the fracturing fluid and the shale at a certain temperature and pressure.

2.4. Analytical methods

Previous analysis of the core samples from this shale gas development zone suggested that the clay minerals mainly consisted of montmorillonite, illite, and kaolinite, and the montmorillonite presented maximal ion-exchange capacity [19]. Fig. 3 was developed to describe the injected and flowback process of fracturing water and the exchange process of Ba^{2+} and other cations. This work should be taken into account from the aspect of ion exchange when fracturing water flow into rock layer and then diffuse to soil. We assumed that the Na$^+$/Ba^{2+}, K$^+$/Ba^{2+}, and Ca^{2+}/Ba^{2+} exchange reactions after the fracturing fluid flows into underground strata are the main sources of Ba^{2+} in the flowback water. Then we calculated Na$^+$/Ba^{2+}, K$^+$/Ba^{2+}, and Ca^{2+}/Ba^{2+} exchange reaction capacities, respectively, based on the rule of equivalent exchange [13]. To verify this prediction, the calculated process and results are given in detail in the next chapter.

The pseudo homogeneous dispersion model and shrinking core model are the most common types of ion-exchange kinetic models [20,21]. Fig. 4 describes the exchange mechanism of the shrinking core model that asserts that ion exchange happens progressively at the unreacted core surface after ions enter the reaction shell side [22]. In this paper, we use the shrinking core model as the low porosity of the clay mineral, which delivers the following assumptions [17,23]:

- Montmorillonite is considered as the rigid sphere of the constant size and volume.
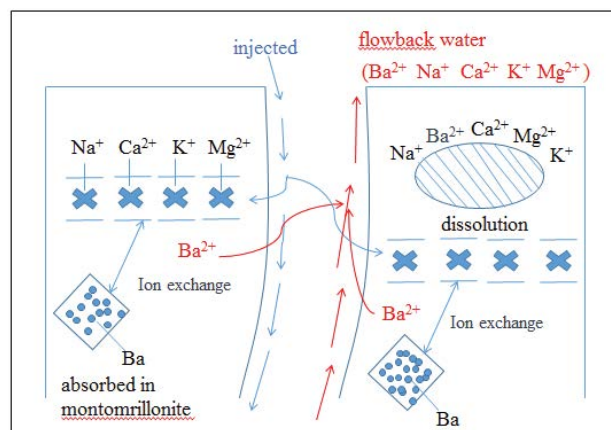
Fig. 3. Possible mechanisms contributing to the production of flowback water cation composition.
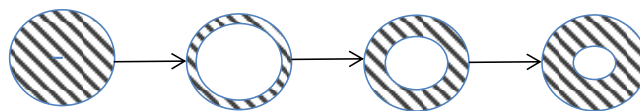
Fig. 4. Shrinking core model.

- There is a "traveling interface" between the reaction and unreacted regions in montmorillonite.
- Exchange capacity is a fixed value.
- The ion-exchange reaction rate is controlled continuously by three processes: liquid film diffusion, particle diffusion, and chemical reaction.
- The chemical reaction rate is much faster than the ion diffusion rate.

3. Results and discussion

3.1. Ion-exchange process

3.1.1. Ion concentrations in flowback water

Fig. 2 shows that the cation concentrations generally increased with time, which proves the solid-liquid reaction between the fracturing fluid and underground minerals [24]. The concentrations of Na^+, K^+, and Ca^{2+} kept increasing within the first 5 d up to 3,905, 4,951, and 190 mg/L, respectively, which indicates that ion-exchange reactions were not observed. After the fifth day, the three ion concentrations decreased at the same time, which indicates the existence of an exchange reaction between Na^+, K^+, and Ca^{2+} with Ba^{2+}. After the seventeenth day, the concentration of these three ions decreased again, which proves that the exchange reactions appeared again. Given the low concentrations and small variations in Mg^{2+}, the influence of Mg^{2+} in the exchange capacity was neglected. Therefore, the exchange capacities of Na^+, K^+, and Ca^{2+} reacting with Ba^{2+} over a period of 25 d were calculated, and the amount of Ba^{2+} released was determined on the basis of equivalent exchange. Table 3 shows that the concentrations of Na^+, K^+, and Ca^{2+} changed with time during the period from Days 5 to 25.

At the beginning of the period from Days 5 to 17, the concentrations of Na^+ and Ca^{2+} decreased to the minimum values on the seventh day, while the concentration of K^+ decreased to the minimum value on the sixth day, which indicated that the K^+/Ba^{2+} reaction rate was the fastest according to Onken's study [10]. The correctness of our previous prediction was proved decisively. The concentrations of Na^+, K^+, and Ca^{2+} decreased by 70, 75, and 10 mg/L over 3 d, respectively. The highest exchange capacity of K^+ took the shortest exchange time while the exchange capacity of Na^+ was slightly less, but the exchange time was more than that of K^+. The exchange capacity of Ca^{2+} was far less compared with K^+ and Na^+, and the exchange time was more than K^+. Thus, the order of the reaction rate was $K^+ > Na^+ > Ca^{2+}$.

During the period from Days 17 to 25, the concentrations of Na^+, K^+, and Ca^{2+} decreased to the minimum values on Day 22, which indicates that there was a lower exchange rate in the later period than in the previous period. This result might be caused by the inadequate capability of ion exchange that was caused by the dissolution of partial montmorillonite in the initial time. The fact that the concentrations of Na^+, K^+, and Ca^{2+} decreased by 45, 51, and 9 mg/L over 5 d, respectively, indicates that the exchange capacities in the later period decreased obviously compared with those in the initial period, but the order of the reaction rate remained the same as mentioned earlier.

3.1.2. Ion-exchange capacity

Based on the rule of equivalent exchange, the ion-exchange reactions between Ba^{2+} adsorbed on montmorillonite, M^+, and M^{2+} in the fracturing fluid can be defined as follows:

$$Montmorillonite - Ba^{2+} + 2M^+ = Montmorillonite - 2M^+ + Ba^{2+}$$

$$Montmorillonite - Ba^{2+} + M^{2+} = Montmorillonite - M^{2+} + Ba^{2+}$$
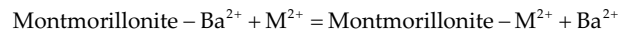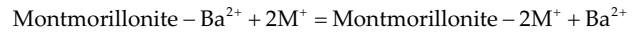
where M^+ refers to Na^+ and K^+ and M^{2+} refers to Ca^{2+}.

Table 4 summarizes the ion-exchange capacities of Na^+, K^+, and Ca^{2+} based on the data in Table 3 and Eq. (4).

In this study, the settling velocity of $BaSO_4$, which is extremely insoluble, was much higher than that of $SrSO_4$ [25], whereas the amount of $SrSO_4$ could be considered negligible. Thus, Ba^{2+} is suggested to be precipitated with SO_4^{2-} during the period from Days 5 to 25. The Ba^{2+} consumption of $BaSO_4$ precipitation was determined on the basis of the mass conservation equation. As shown in Table 4 and Fig. 2(e), the following results were calculated: (1) during the period from Days 5 to 17, the production of Ba^{2+} was 374.01 mg/L and the consumption of SO_4^{2-} and Ba^{2+} was 170 and 242.6 mg/L, respectively, and (2) during the period from Days 17 to 25, the production of Ba^{2+} was 236.32 mg/L and the consumption of SO_4^{2-} and Ba^{2+} was 75 and 107.03 mg/L, respectively. Therefore, the concentration of Ba^{2+} increased by 131.41 mg/L during the first period from Days 5 to 17, and it increased by 129.29 mg/L during the second period from Days 17 to 25.

The calculated results show that the concentration of Ba^{2+} increased by 260.7 mg/L in the flowback water within 25 d, while the engineering data show that it increased by 265 mg/L, which was a little higher. This might be because a part of the barium came from mineral dissolution or other

Table 3
Concentrations of Na^+, K^+, and Ca^{2+} with time

Concentration (mg/L) Time (day)		Na^+	K^+	Ca^{2+}
Initial 5th–17th	5	3,905	4,951	190
	6	3,871	4,876	187
	7	3,835	5,120	180
Later 17th–25th	17	10,050	12,100	430
	22	10,005	12,049	426

Table 4(a)
Ion-exchange capacities of Na^+, K^+, and Ca^{2+} during 5th to 17th day. $\dfrac{meq}{g} = \dfrac{mg}{g} \times \dfrac{valence}{atomic\ weight}$

Time	Cations	Ion-exchange capacities (meq/g)
Initial 5th–17th day	Na^+	0.0304
	K^+	0.0192
	Ca^{2+}	0.0050

Table 4(b)
Ion-exchange capacities of Na^+, K^+, and Ca^{2+} during 17th to 25th day

Time	Cations	Ion-exchange capacities (meq/g)
Later 17th–25th day	Na^+	0.0195
	K^+	0.0130
	Ca^{2+}	0.0020

chemical reactions and the dissolved barium in the fracturing fluid returned to the surface as flowback water. However, its production was much smaller than ion-exchange production.

We made a comparison between the engineering data and the theoretically calculated data of Ba^{2+}. Fig. 5 shows that the theoretical calculations are in good agreement with the engineering results for Ba^{2+}. Therefore, we derive the important conclusion that the ion-exchange reaction is the main reason for the increase in Ba^{2+}. We do not discount the possibility that dissolution and other chemical reactions are secondary reasons which control the concentration increase of Ba^{2+}.

The main reason for the increase in Ba^{2+} has been confirmed as the ion-exchange reaction, so Table 5 shows the rates of the Na^+, K^+, and Ca^{2+} exchange with Ba^{2+}.

The maximum concentration of Na^+ and K^+ was about 13,000 mg/L and that of Ca^{2+} was 590 mg/L in the flowback water. Table 5 shows that the proportion of M^+/Ba^{2+} exceeded 80%; thus, Ba^{2+} mainly exchanged with monovalent cations and then contributed more exchange capacities. Next, Ba^{2+} exchanged with divalent cations. The average exchange capacities of Na^+, K^+, and Ca^{2+} were 53.98%, 35.06%, and 7.15%, respectively. Other chemical reactions and dissolution accounted for 3.81% in 25 d.

From the above, the ion-exchange reaction was the main source of Ba^{2+}.

3.2. Kinetic model of ion exchange

The previous chapters indicated that barium ion mainly came from ion exchange. However, given the complicated underground strata [26] and polytropic compositions of the fracturing liquid, it is difficult to accurately constrain each ion-exchange reaction rate. Research on the exchange process of Ba^{2+} based on ion-exchange kinetics could be acceptable. Liquid film diffusion, particle diffusion, and chemical reaction are the main steps of the exchange rate, so one of these can limit the reaction rate. The shrinking core model was used in this study, and the equations are as follows [20]:
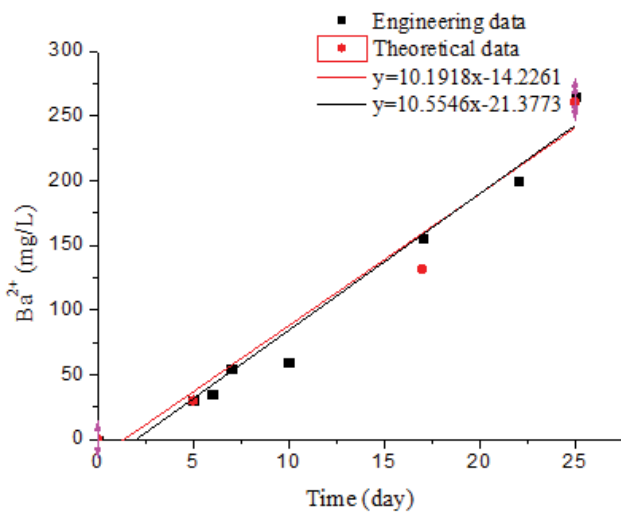
Fig. 5. Comparison between engineering data and theoretical data of Ba^{2+}.

Table 5(a)
Rates of Na^+, K^+, and Ca^{2+} exchange during the initial time

Time	Cation	Rate (%)
Initial 5th–17th day	Na^+	52.41
	K^+	33.10
	Ca^{2+}	8.62

Table 5(b)
Rates of Na^+, K^+, and Ca^{2+} exchange at a later time

Time	Cation	Rate (%)
Later 17th–25th day	Na^+	55.55
	K^+	37.03
	Ca^{2+}	5.69

Liquid film diffusion: $F = \dfrac{3C_0 K_f}{a Q_r}$ (1)

Particle diffusion: $1 - 3(1-F)^{2/3} + 2(1-F) = \dfrac{6DC_0}{a Q_r^2} t = kt$ (2)

Chemical reaction: $1 - (1-F)^{1/3} = \dfrac{K_c C_0}{r} t$ (3)

The key step of the reaction could be calculated by using Eqs. (1)–(3).

The ion-exchange capacity and exchange degree could be defined as follows:

$$Q = \frac{(C_0 - C)}{M} \times V$$ (4)

$$F = \frac{Q_t}{Q_\infty}$$ (5)

where C_0 is the initial concentration of ion in aqueous solutions, C is the ion concentration in exchange equilibrium, V is the aqueous volume, M is the quality of ion-exchange resin, and v/m is 10^{-2} in this study [7]. Q_t is the ion-exchange capacity at time t, and Q_∞ is the ion-exchange capacity at equilibrium.

The detection results show that the concentrations of Ba^{2+} were 270 and 30 mg/L at Days 27 and 5, respectively. Hence, Q was 2.4 mg/g. Table 6 shows the kinetic calculated data of Ba^{2+} by using Fig. 2(d) and Eqs. (1)–(5).

The curves of F, $1-3(1-F)^{2/3} + 2(1-F)$, and $1-(1-F)^{1/3}$ changed with time and are described in Fig. 6 on the basis of the calculated results summarized in Table 6 to clarify the controlling step of the ion-exchange rate.

Fig. 6 shows that the relationship between F and t was linear, while the relationships between the values of

Table 6
Data of ion-exchange kinetics

Time (d)	Ba^{2+} (mg/L)	Q_t	F	$1–3(1–F)^{2/3} + 2(1–F)$	$1–(1–F)^{1/3}$
5	30	2.4	1	1	1
10	60	2.05	0.8723	0.4946	0.4964
17	155	1.1	0.4583	0.0898	0.1848
20	200	0.65	0.2708	0.028	0.0999
25	265	0.05	0.0213	0.00015	0.0072
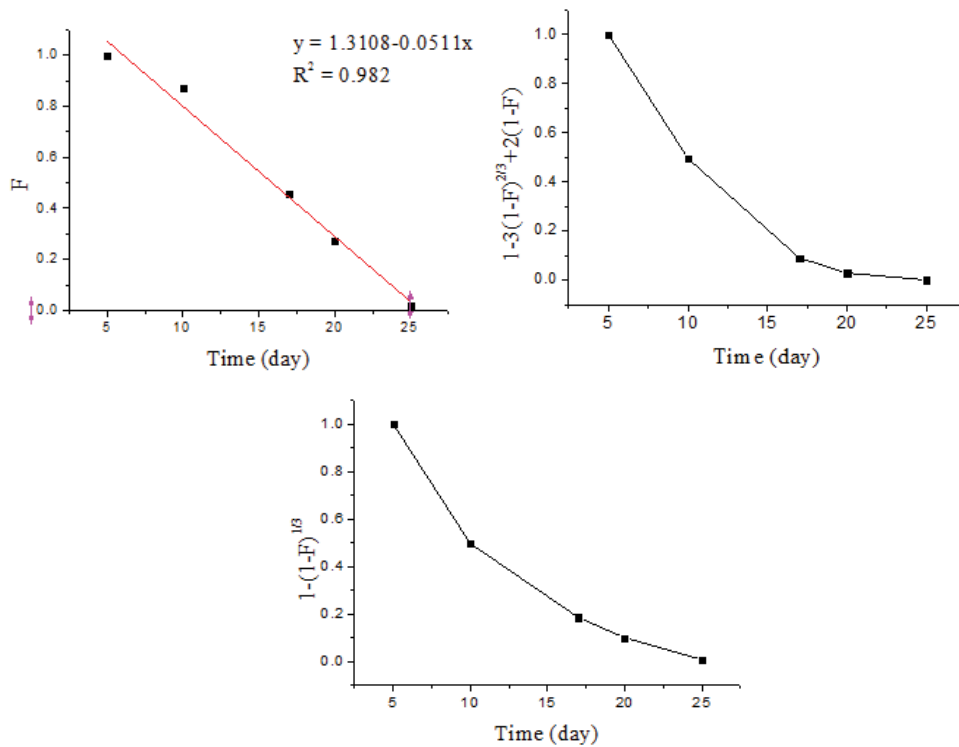
Fig. 6. Relation diagrams of $F(t) − t$, $[1–3(1–F)^{2/3} + 2(1–F)] − t$ and $[1–(1–F)^{1/3}] − t$.

$1–3(1–F)^{2/3} + 2(1–F)$, $1–(1–F)^{1/3}$, and t were nonlinear. It mainly indicates that the ion-exchange rate was neither controlled by particle diffusion nor chemical reaction but by liquid film diffusion.

4. Conclusion

By focusing on the production of barium ion, the research calculated the Ba^{2+} exchange capacity and exchange process based on ion-exchange kinetics. The following results could be known:

• This research discussed two sources for the increased concentration of Ba^{2+} in flowback water. We confirmed that one source was the Na^+/Ba^{2+}, K^+/Ba^{2+}, and Ca^{2+}/Ba^{2+} exchange reactions produced Ba^{2+}. The calculated results presented a high fitting degree with engineering data, and the results showed that the ion-exchange capacities of Na^+, K^+, and Ca^{2+} were 53.98%, 35.06%, and 7.15%, respectively. Thus, the ion-exchange reaction was the main source for increased Ba^{2+}. In addition, the source of partial Ba^{2+} possibly came from dissolution or other chemical reactions, and the mechanism needs further study.

• The results of fitting the ion-exchange degree with time on the basis of shrinking core model showed that the fitting degree of $F(t) – t$ was the highest and the value was 0.982, which indicated that the Na^+/Ba^{2+}, K^+/Ba^{2+}, and Ca^{2+}/Ba^{2+} reaction efficiencies were controlled by liquid film diffusion.

References

[1]	A.J. Calderón, O.J. Guerrab, L.G. Papageorgiou, G.V. Reklaitis, Disclosing water-energy-economics nexus in shale gas development, Appl. Energ., 225 (2018) 710–731.

[2]	D. Rahm, Regulating hydraulic fracturing in shale gas plays: the case of Texas, Energ. Policy, 39 (2011) 2974–2981.

[3]	W.A.M. Wanniarachchi, P.G. Ranjitha, M.S.A. Perer, T.D. Rathnaweer, D.C. Zhang, C. Zhang, Investigation of effects of fracturing fluid on hydraulic fracturing and fracture permeability of reservoir rocks: an experimental study using water and foam fracturing, Eng. Fract. Mech., 194 (2018) 117–135.

[4]	J.-x. Liu, Present situation of the treatment of shale gas fracturing flowback fluid, Contemp. Chem. Ind., 45 (2016) 1671–0460.

[5]	D.L. Shaffer, L.H.A. Chavez, M. Bensasson, R.V. Castrillón, Desalination and reuse of high-salinity shale gas produced water: drivers, technologies, and future directions, Environ. Sci. Technol., 47 (2013) 9569–9583.

[6]	S.M. Dischinger, J. Rosenblum, R.D. Noble, D.L. Gin, K.G. Linden, Application of a lyotropic liquid crystal nanofiltration membrane for hydraulic fracturing flowback water: selectivity and implications for treatment, J. Membr. Sci., 543 (2017) 319–327.

[7]	D. Renock, J.D. Landis, M. Sharma, Reductive weathering of black shale and release of barium during hydraulic fracturing, Appl. Geochem., 65 (2015) 73–86.

[8]	B.W. Stewart, E.C. Chapman, R.C. Capo, J.D. Johnson, J.R. Graney, C.S. Kirby, K.T. Schroeder, origin of brines, salts and carbonate from shales of the Marcellus formation: evidence from geochemical and Sr isotope study of sequentially extracted fluids, Appl. Geochem., 60 (2015) 78–88.

[9]	T.T. Phan, R.C. Capo, B.W. Stewart, J.R. Graney, J.D. Johnson, S. Sharma, J. Tora, Trace metal distribution and mobility in drill cuttings and produced waters from Marcellus shale gas extraction: uranium, arsenic, barium, Appl. Geochem., 60 (2015) 89–103.

[10]	A.B. Onken, R.L. Matheson, Soil science, J. Acoust. Soc. Am., 46 (1982) 276–279.

[11]	Y. Liu, G. Hongkui, C. Yuanfang, Investigation on fracturing fluid imbibition-ion diffusion and its influencing factors in shale reservoirs, China Offshore Oil Gas, 28 (2016) 94–99.

[12]	X. Wang, Q. Wang, An experimental study on rock/water reactions for alkaline/surfactant/polymer flooding solution used at Daqing, Oilfield Chem., 20 (2003) 250–253.

[13]	Y.-x. Wen, Ion-exchange kinetics of Mg^{2+}–NH^{4+} of waste solution from demagging of phosphorus ore, J. Sichuan Univ., 32 (2000) 101–104.

[14]	M. Li, W. Yang, M. Xin, Kinetics of the Na^+–Cu^{2+} ion exchange on the Na-form clinoptilolite, Acta Phys. -Chim. Sin., 13 (1997) 224–228.

[15]	P.C.C. Siu, L.F. Koong, J. Saleem, J. Barford, G. McKay, Equilibrium and kinetics of copper ions removal from wastewater by ion exchange, Chin. J. Chem. Eng., 24 (2016) 94–100.

[16]	Z.A. AlOthman, M.M.l. Alam, Mu. Naushad, Heavy toxic metal ion exchange kinetics: validation of ion exchange process on composite cation exchanger nylon 6,6 Zr(IV) phosphate, J. Ind. Eng. Chem., 19 (2013) 956–960.

[17]	Y. Wu, Synthesis of MnO_2-type potassium ion-sieve and study on ion exchange action for K+, Qingdao University of Science and Technology, Qingdao, China, 2008, pp. 49–54.

[18]	T.T. Phana, A.N. Paukert Vankeuren, J.A. Hakala, Role of water–rock interaction in the geochemical evolution of Marcellus Shale produced waters, Int. J. Coal Geol., 191 (2018) 95–111.

[19]	H. He, An experimental study of adsorption capacity of montmorillonite, kaolinite and illite for heavy metals, Actapetrologica et mineralogica., 20 (2001) 573–577.

[20]	Z. Jiang, Ion exchange kinetics and application (1), Ion Exchange Adsorpt., 5 (1989) 54–73.

[21]	Z. Jiang, Ion exchange kinetics and application (2), Ion Exchange Adsorpt., 5 (1989) 221–233.

[22]	Z. Qin, Study on ion-exchange kinetics, Tianjing University, Tianjing, China, 2004, pp. 4–10.

[23]	S.S. Razavi-Tousi, J.A. Szpunar. Modification of the shrinking core model for hydrogen generation by reaction of aluminum particles with water, Int. J. Hydrogen Energy, 41 (2016) 87–93.

[24]	X. Tian, Simulation of fracturing fluid-methane-minerals interactions during hydraulic fracturing of shale gas, China University of Geosciences, Wuhan, China, 2015, pp. 13–38.

[25]	C. He, M. Li, Kinetics and equilibrium of barium and strontium sulfate formation in Marcellus shale flowback water, J. Environ. Eng., 140 (2014) 1943–7870.

[26]	J.N. Williams, V.G. Toy, S.A.F. Smith, C. Boulton, Fracturing, fluid-rock interaction and mineralisation during the seismic cycle along the Alpine Fault, J. Struct. Geol., 103 (2017) 151–166.